Evaluation of open-access global digital elevation models (AW3D30, SRTM and ASTER) for flood modelling purposes

Laurent Guillaume Courty[a, b], Julio Cesar Soriano-Monzalvo[a, b], and Adrián Pedrozo-Acuña[a,*]

[a]Instituto de Ingeniería, Universidad Nacional Autónoma de México, Circuito Escolar, Ciudad Universitaria, Coyoacán, 04510, Ciudad de México, Mexico
[b]Programa de Maestria y Doctorado en Ingeniería, Universidad Nacional Autónoma de México, Circuito de Posgrado, Ciudad Universitaria, Coyoacán, 04510, Ciudad de México, Mexico
[*]Correspondance to: apedrozoa@ii.unam.mx

August 2017

Keywords: Digital Elevation Model, flood, ALOS.

Abstract

Elevation data in the form of Digital Elevation Models (DEMs) has been recognised as a basic piece of information for the accurate representation of topographic controls exerted in hydrologic and hydraulic models. Yet many practitioners rely on open-access global datasets usually obtained from space-borne survey due to the cost and sparse coverage of sources of higher resolution. In may 2016 the Japanese Aerospace eXploration Agency (JAXA) publicly released an open-access global DEM at an horizontal resolution of 30 m, the ALOS World 3D-30m (AW3D30). So far no published study assessed the flood modelling capabilities of this new product. The purpose of this investigation is twofold. Firstly, to present an assessment of the capacity of the AW3D30 DEM for flood modelling purposes and secondly, to compare its performance with regards to computed water levels and flood extent maps calculated using other freely available 30 m DEMs for model setup (e.g. SRTM and ASTER GDEM). For this comparison, the reference to reality is given by the water levels and flood extent maps computed with the same numerical model but using a LiDAR based DEM (5 m of spatial resolution re-sampled to 30 m). The numerical model employed in this investigation is based on a damped partial inertia approximation of the Saint-Venant equations on a regular raster grid, which is forced with a simple and synthetic rainfall storm event. Numerical results using different elevation data in model setup are compared for two regions with contrasting topographic gradients (steep and smooth). Results with regards to water depth and flood extent show that AW3D30 DEM performs better than the SRTM DEM. Notably, in the case of mountainous regions results derived with the AW3D30 DEM are comparable in skill to those obtained with a LiDAR derived DSM, suggesting its suitability in the numerical reproduction of flood events. This encouraging performance paves the way to more accurate modelling for both data-scarce regions and global flood models.

1 Introduction

Inundations are the disasters that affect more people in the world [IFRC, 2016]. In the future and under conditions driven by climate change, the population exposed to floods is likely to increase [Hirabayashi et al., 2013]. Hallegatte et al. [2013] predict that without improvement in flood defences, the flood-related damages in coastal cities alone could reach US$1 trillion a year by 2050.

It is acknowledged that in order to assess the level of exposure to these hydrometeorological events, it is necessary to apply hydraulic models that resolve the fundamental equations of the physics to describe the physics of the water overflowing from riverbanks; usually, these equations

may be resolved in one or more Cartesian dimensions. However, as the level of complexity of these numerical tools increases, the data requirements for the model setup also increase.

On the other hand, given the recent diffusion of remotely sensed data for both hydrological variables (e.g. precipitation [Hou et al., 2014]) and topographic information [Sanders, 2007], has enabled an evolution on the level of sophistication of numerical tools and approaches used by hydrologists, favouring the use of bidimensional models [Bates, 2004].

Among the most important datasets that are needed to carry out a proper flood inundation modelling exercise, are hydrometeorological observations (i.e. rating curves, rainfall, runoff) to define boundary and initial conditions, topographic data for the description of the catchment geometry, and flood extent maps or high flood marks for model calibration and validation [Di Baldassarre]. Evidently, the level of accuracy and resolution in all these datasets have an effect on the reliability of the model results. For instance, in the case of topographic data, a commonly used input is the Digital Elevation Model (DEM), which represents a gridded product with values of elevation. This was actually proved in a numerical exercise presented by Horritt and Bates [2001], whom showed that inundation models of large rivers have a maximum performance at a spatial resolution of 50 m. Their numerical results were compared in terms of identified affected areas against those detected by satellite imagery. Indeed, there is a wide recognition that accurate DEMs are critical for accurate flood modelling and management [Bates, 2004, Cook and Merwade, 2009].

DEMs are often derived using remote sensing techniques, such as Light Detection and Ranging (LiDAR) surveys. These airborne laser altimetry datasets, enable a numerical description of the floodplains with planimetric resolution of 1 m and finer. Therefore, along with the use of Geographic Information Systems (GIS), its use has encouraged the utilisation of bidimensional hydraulic models in flood modelling studies [Marks and Bates, 2000, Sanders, 2007]. In the last 20 years, the development of aerial lidar has been a game-changer in the field of flood modelling thanks to its ability to quickly survey large areas at relatively high vertical accuracy [Hodgson and Bresnahan, 2004] and spatial resolution. However, in some countries, its utilisation has not been widespread due to its high cost.

On the other hand, there has also been a clear improvement in the availability of space-borne topographic data that are global and free. Indeed, recent studies report the use of this type of datasets to support flood modelling activities [Jarihani et al., 2015, Yan et al., 2015a,b].

This is the case of the Shuttle Radar Topography Mission (SRTM), which in the first decade of this century produced a global dataset with a spatial resolution of 3″ (around 90 m) [Farr et al., 2007]. This dataset was acquired using Interferometric Synthetic Aperture Radar (InSAR) during an 11 days mission aboard the NASA space shuttle in February 2000, while the first version of the DEM was released in 2003 covering an area of Earth between 60° north and 56° south. The availability this SRTM DEM made it one of the most commonly used global DEM for hydraulic and hydrologic modelling of large rivers [Schumann et al., 2010]. For instance, LeFavour and Alsdorf [2005] demonstrated its application to derive useful hydraulic parameters in the Amazon river, such as water surface slope and discharge. Although it is still recognised that the dataset has a low accuracy (around 6 m), the data have proven to be of great use for flood modelling studies, especially in cases where detailed topographic data (e.g. LiDAR) are not available [Pedrozo-Acuña et al., 2012, 2015]. More recently, during 2015, the US government released a new version of the global SRTM DEM with an improved spatial resolution of 30 m.

Additionally, another well-known global and free dataset for elevation is that produced by a cooperation of the Ministry of Economy, Trade, and Industry (METI) of Japan and the NASA. This product known as ASTER GDEM [Tachikawa et al., 2011] was created using data from the Advanced Spaceborne Thermal Emission and Reflection Radiometer (ASTER) image instrument aboard the Terra satellite. The version 1 was released in 2009 and the version 2 in 2011. The latter version employs data collected between 2000 and 2010, covering the earth surface between 83° north and 83° south while its horizontal resolution is around 30 m at the equator. Several authors compared the ASTER GDEM in its version 2 to ground control points on various continents and found RMSE of 8 m to 13 m [Gesch et al., 2014, Rexer and Hirt, 2014, Jing et al., 2014, Santillan and Makinano-Santillan, 2016]. Due to its lower accuracy than the SRTM, the application of ASTER DEMs in flood modelling is sparse, with only few examples of successful utilisation [e.g Tarekegn et al., 2010, Wang et al., 2012].

The latest addition of open-access global DEMs is the ALOS World 3D-30m (AW3D30) [Tadono et al., 2016] released in May 2016 by the Japan Aerospace Exploration Agency (JAXA). It as been

created by using the images of the PRISM panchromatic stereo mapping sensor on board the Advanced Land Observing Satellite (ALOS). This open-access DEM is a resample of a commercial 5 m Digital Surface Model (DSM). It covers an area roughly between 82° north and 82° south. Due to its novelty, the utility of this dataset in flood modelling has not yet been tested.

In contrast, multiple studies have presented comparisons of the accuracy and differences between the elevation data from SRTM and ASTER GDEM, and found that the former performs generally better than the latter [Hirt et al., 2010, Jing et al., 2014, Gesch et al., 2014, Rexer and Hirt, 2014, Jarihani et al., 2015]. To the best of our knowledge, the article of Santillan and Makinano-Santillan [2016] is the only independent study that evaluates the quality of AW3D30 DEM. Indeed, this study presents a comparison of the 30 m version of SRTM, AW3D30 and ASTER GDEM2 to ground measurements over the Philippines. Their results indicated that for this region, the AW3D30 presented the lowest errors followed by the SRTM and then the ASTER GDEM2. Moreover, Yamazaki et al. [2017] presented an error-corrected DEM that uses the AW3D30 for filling missing values identified in the SRTM dataset. However, the article does not provide a comparison between those two datasets. While the work of Santillan and Makinano-Santillan [2016] shows that the AW3D30 gives encouraging results from the point of view of absolute altitude accuracy, it does not go as far as evaluating the DEMs for hydrologic and hydraulic applications.

Given the proved utility and the new availability of these datasets, the objective of this study is twofold. Firstly to present an assessment of the capacity of the AW3D30 DEM for computer flood modelling and secondly, to compare its performance with regards to computed water levels and flood extent maps calculated using other freely available 30 m DEMs for model setup (e.g. SRTM and ASTER GDEM). For this comparison, the reference to reality is given by the water levels and flood extent maps computed with the same numerical model but using a LiDAR based DEM (5 m of spatial resolution re-sampled to 30 m). The numerical model utilised in this study is a GIS-integrated, open-source dynamic hydrologic and hydraulic model known as Itzï Courty et al. [2017], which solves a damped partial inertia approximation of the Saint-Venant equations on a regular raster grid [de Almeida et al., 2012, de Almeida and Bates, 2013]. The comparison is carried out in two urban catchments located in Mexico, with contrasting topographic gradients (steep and flat).

This paper is organised as follows, Section 2 introduces the details of the different DEMs that are utilised, the study areas and the type of evaluation we perform. Section 3 describes the results we obtained and Section 4 presents a discussion of the implications of results in the context of flood modelling. Finally, Section 5 summarises the main conclusions found in this investigation.

2 Material and methods

2.1 Study areas

Two different catchments with important urban areas are selected for the comparison of model results. The numerical description of both catchments is constructed using the different freely available 30 m DEMs (e.g. AW3D30, SRTM and ASTER GDEM).

The urban areas correspond to Saltillo in the state of Coahuila and Reynosa in the state of Tamaulipas, both in the northeastern part of the country. Fig. 1 introduces the geographic location of both cities. Watersheds have been defined to cover the majority of the urban areas, while the urban areas are taken from the database of the National Commission for the Knowledge and Use of the Biodiversity of Mexico (CONABIO).

Both catchments represent terrains and catchments with contrasting physiographies and characteristics. While Saltillo is located in a mountainous region, Reynosa is mainly characterised by flat and low-lying region. Moreover, Table 1 introduces the contrasting characteristics for both cities such as: catchment area, number of raster cells involved in each case, urban area, maximum, minimum and mean slope of the terrain and the corresponding concentration times for both cases. From the comparison of these values, it is clear that Saltillo represents a larger test case with a with a quicker rainfall-runoff response in the catchment in comparison to the values reported for Reynosa.

The urban area of Reynosa includes the municipalities of Reynosa and Río Bravo. The catchment is located at the border with the United States of America, in the valley of the Río Bravo river. The watershed includes artificial irrigation structures that initiate at the Anzaldúas dam on the Río Bravo river upstream Reynosa. The Anzaldúas canal cross Reynosa and then pass south

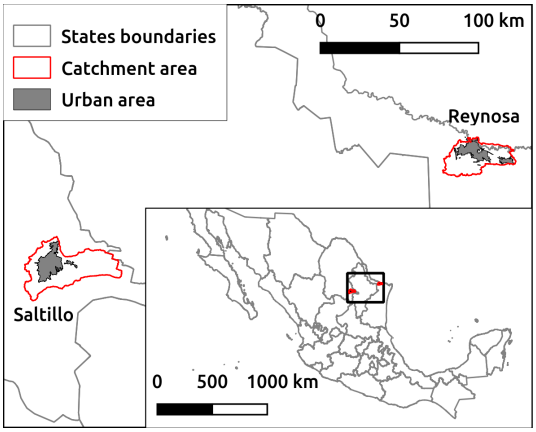

htp

Figure 1: Location of the study areas in Mexico.

of the city of Río Bravo. The Retamal canal branches out of the Anzaldúas canal after Reynosa and circumvent the city of Río Bravo on the north. Those canals are equipped with sluice gates that further modify the natural hydrology of the catchment.

In the case of Saltillo, the urban area includes the municipalities of Ramos Arizpe, Arteaga and Saltillo proper. Most of the built up area lies in a valley on the west of the Sierra Madre Oriental mountain range. The main mountainous area is on the east of the watershed and consists of the Sierra la Martha mountain that culminates at the Cerro San Rafael more than 3700 m above sea level.

Table 1: Informations of the study areas. The population of the urban areas are from INEGI (Reynosa 2015, Saltillo 2010), the elevations and slopes are from the lidar DTM.

	Reynosa	Saltillo
Population	≈773 000	≈923 000
Catchment area (km^2)	683	1188
#Raster cells	1 273 580	2 745 792
Urban area (km^2)	174.7	229.0
Min. elevation (m)	20	1299
Max. elevation (m)	152	3711
Max. slope (°)	17.9	70.9
Mean slope (°)	0.75	13.75
Median slope (°)	0.5	8.5
t_c (Kirpich, in hours)	19.5	8.5

2.2 Elevation data

Elevation data in the form of DEMs have been recognised as a basic piece of information for the accurate representation of topographic controls exerted in both, hydrologic [Kenward, 2000] and hydraulic models [Cobby et al., 2001, Meesuk et al., 2015]. This is more true in urban environments, where LiDAR derived DEMs have been recognised as the best possible source of elevation data [Fewtrell et al., 2008, Gallegos et al., 2009]. Therefore, in this investigation, LiDAR derived DEMs are used as a reference to reality.

LiDAR derived DEMs are obtained from the National Institute for Statistic and Geography of Mexico (INEGI). In both case studies, two different LiDAR products are utilised with a horizontal resolution of 5 m. The first one corresponds to a digital surface model (DSM), which is based on first echoes with threes, buildings etc., while the second is a digital terrain model (DTM) where all these features have been removed to obtain a bare-earth model.

For a fair comparison of LiDAR derived DEMs against the global DEMs of coarser spatial resolution, both LiDAR products are re-sampled to 30 m to compare results related to the same spatial resolution. The up-scaling of this information is performed using an arithmetic mean

aggregation method, and the reference to reality is given by the numerical results obtained using the LiDAR derived DTM model.

With regards to the global DEMs, we utilise the AW3D30, the SRTM1, the ASTER GDEM all of which have a spatial resolution of $1''$. Although some studies have presented comparisons and validations of the SRTM and ASTER global DEMs either for flood modelling [Tarekegn et al., 2010, Jarihani et al., 2015, Jing et al., 2014] or vegetation correction [O'Loughlin et al., 2016]. Our investigation is timely due to the lack of information with regards to the usability of the AW3D30 DEM for flood modelling purposes.

Table 2 introduces the geographic information related to the different DEMs used in this study. All DEMs have been projected to a common coordinate system, the Mexico ITRF2008/LCC (EPSG 6372) using GRASS GIS with a bilinear interpolation. It should be noted that in order to assess the potential of each elevation product, we carry out as few processing as possible.

Table 2: Geographic information of the raw elevation data.

Product	Coord. system	Hor. datum	Vert. datum	Hor. resolution
LIDAR	UTM14N	ITRF92	NAVD88	5 m
AW3D30	lat/long	WGS84	EGM96	$1''$
SRTM1	lat/long	WGS84	EGM96	$1''$
ASTER GDEM2	lat/long	WGS84	EGM96	$1''$

With regards to the global DEMs we utilise the first version of the SRTM with a resolution of $1''$, while the ASTER GDEM corresponds to the second version of the product. Both datasets are downloaded from the USGS EarthExplorer service.

In the case of the AW3D30 DEM, we employ the version 1 downloaded from the official JAXA web page. This dataset is an up-scaling of the ALOS World 3D commercial DEM with spatial resolution of 5m. It should be noted that for this dataset, two versions of the data are distributed, which depend on the aggregation method used during the re-sampling: mean or median. In this investigation, we use the data obtained by the arithmetic mean method. In both cities, this dataset was checked for voids. In Saltillo, the data was completely covered with valid data of high correlation. While in the case of Reynosa, the dataset presented a 0.1 % of voids and 0.57 % of pixels identified as land water and low correlation. The low percentage of voids in the data was replaced using an interpolation filling technique based on the regularised spline with tension [Mitášová and Mitáš, 1993].

2.3 Comparison of slope and aspect

Table 2 reports that DEMs selected in this study have different vertical reference systems. In the case of LiDAR derived datasets, INEGI maintains a network of land survey benchmarks in yet another datum (NAVD29). This makes difficult the comparison of absolute altitudes between DEMs.

Furthermore, the absolute altitude is a poor indicator of a DEM's capacity for flood simulations. For this reason, we decided not to perform a comparison of altitude. Instead, the relative altitude difference between cells (i.e. slope and aspect), is implemented. This characteristic is of better help when the evaluation of a DEM for flood modelling is sought. Indeed, most of the physically-based flood models, including the one used in this paper, rely on the altitude differences between two raster cells to calculate the flow. Therefore, the absolute accuracy of the elevation above the mean sea level is of little help to evaluate the quality of a DEM for flood modelling.

Following Sampson et al. [2016], physical characteristics derived from the LiDAR derived DTM are used as reference, as the *bare-earth* model is considered the best suited for flood modelling.

In the case of very smooth slopes and to prevent errors in aspect calculation, the minimum slope to undertake this mathematical operation is set to $0.02°$. Otherwise, the aspect is not evaluated. The aspect map represents the direction in degrees counter-clockwise from east, which the slope is facing. The angle error $\Delta\phi$ is calculated using Eq. 1, where ϕ_1 and ϕ_2 are the compared angles.

$$\epsilon = |(\phi_1 - \phi_2)| \tag{1a}$$

$$\Delta\phi = 180 - |\epsilon - 180| \tag{1b}$$

2.4 Computer model

The numerical tool utilised in this investigation corresponds to a GIS-integrated, open-source dynamic hydrologic and hydraulic model known as Itzï Courty et al. [2017]. This model solves a damped partial inertia approximation of the Saint-Venant equations on a regular raster grid [de Almeida et al., 2012, de Almeida and Bates, 2013].

The time-step duration Δt is calculated at each time-step using Eq. 2, where h_{max} is the maximum water depth within the domain, g the acceleration due to the gravity and α an adjustment factor.

$$\Delta t = \alpha \frac{\min\{\Delta x, \Delta y\}}{\sqrt{g \times h_{max}}} \tag{2}$$

The flow between cells q is calculated with Eq. 3, where subscripts i and t denotes space and time indices, S the hydraulic slope and θ an inertia weighting factor. The flow depth h_f is the difference between the highest water surface elevation y and the highest terrain elevation z. It is used as an approximation of the hydraulic radius.

$$q_{i+1/2}^{t+\Delta t} = \frac{\left(\theta q_{i+1/2}^{t} + (1-\theta)\dfrac{q_{i-1/2}^{t} + q_{i+3/2}^{t}}{2}\right) + g h_f \Delta t S}{1 + g\Delta t n^2 |q_{i+1/2}^{t}| / {h_f}^{7/3}} \tag{3}$$

The water depth at each cell centre is calculated using Eq. 4. It is the sum of the current depth h^t, the external factors h_{ext}^t (rainfall, infiltration, drainage etc.) and the flows passing through the four faces of each cell.

$$h^{t+\Delta t} = h^t + h_{ext}^t + \frac{\sum^4 Q_{i,j}^t}{\Delta x \Delta y} \times \Delta t \tag{4}$$

2.5 Description of numerical flood events

In both selected cities, Saltillo and Reynosa, numerical runs are set up using the different elevation datasets (LiDAR DSM and DTM, ASTER DEM, SRTM1 and AW3D30). This is done in order to calculate water levels and flood extent maps for each city and DEM. Reference to reality is ascribed to those numerical results obtained by using the LiDAR based DTM in the numerical setup.

In order to evaluate solely the influence of the DEM on the model results, we define a synthetic rainfall storm event uniform in space and constant in time at $10\,\mathrm{mm\,h^{-1}}$. Moreover, friction is also considered spatially uniform and is set to a Manning's n coefficient of $0.04\,\mathrm{s\,m^{-1/3}}$. Infiltration and evapotranspiration are neglected. In each case study, the simplicity of the numerical setup enables a careful examination of differences in results, which result from the use of different elevation data.

Additionally, in the case of the city of Reynosa, there is a clear influence of the upstream flow from the Río Bravo, which for the purposes of this investigation is neglected.

Table 3 introduces a summary of the simulation parameters utilised in both cases (Reynosa and Saltillo).

Also in both catchments, downstream boundary conditions are set to allow the outflow of water from the numerical domain. Moreover, the discharge of water flowing through these outflow boundaries is recorded. The simulation time is set to 48 h, which is considered sufficient to allow flow stabilisation in both cases, as this value is bigger than the reported concentration times (See Table 1).

Numerical results with regards to water depths and flood extents are reported in each case. For clarity in the comparison of model results between runs, a numerical threshold to define a flooded element is set to 20 cm. Moreover, the Critical Success Index is estimated to quantitatively determine the model skill with regards to flood extent area.

3 Results

3.1 Comparison of slope and aspect

Figure 2 displays for both cities, the Mean Absolute Error (MAE) in slope and aspect resulting from the comparison of these variables derived for each DEM against those calculated using the LiDAR

Table 3: Simulation parameters

Parameter	Value
α	0.5
Δt_{max} (s)	1.0
θ	0.8
Manning's n ($\mathrm{s\,m^{-1/3}}$)	0.04
Rainfall (mm/h)	10.0

DTM as a reference. It is shown, that all tested DEMs have clear differences when compared against the LiDAR DTM. IN this Figure, bars represent the size of the error where a smaller bar indicates a better performance.

Notably in Saltillo, where the catchment is characterised by steeper gradients, the slope errors are greater than those registered in Reynosa (region with smoother slopes). On the other hand, the aspect errors in the city with stepper gradients (Saltillo) are notably lower than those reported in the smother gradients region (Reynosa). This may be ascribed to the steeper slopes in the former that might prevent changes in aspect due to absolute altitude variation.

Naturally, in these results, the LiDAR derived DSM is the dataset best performance (e.g. smaller errors). Furthermore, the SRTM reports a better accuracy than that reported by the ASTER DEM, which incidentally is the dataset with poorest performance in both cases.

Results estimated in both cities for the AW3D30 DEM, show a better performance of this dataset than that reported by the SRTM DEM. Noticeably, in the steeper gradient region (Saltillo) the MAE of slope reported for the AW3D30 DEM, is nearly two times smaller than that registered for the SRTM DEM. Whereas in the region with smoother slopes (Reynosa), results of MAE in slope show similar performance between both the AW3D30 DEM and the SRTM DEM, with a very small advantage of the latter.

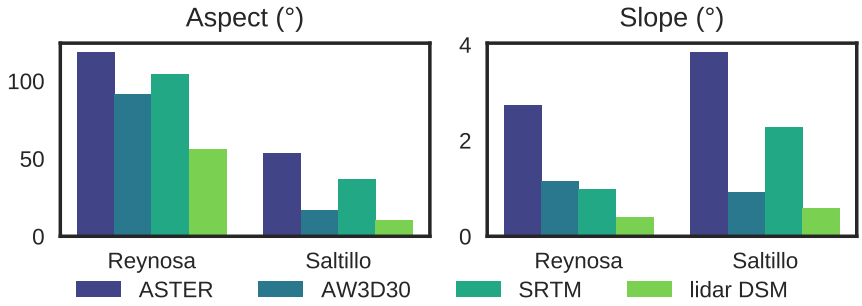

Figure 2: Mean Absdolute Error in slope and aspect of each DEM compared to the lidar DTM. Lower is better.

3.2 Inundation modelling

3.2.1 Numerical stability

Before starting the analysis related to hydrodynamic variables estimated using the different DEMs. In order to make sure that numerical results are usable and comparable, it was determined that a revision of the numerical stability of the simulations was necessary.

Therefore, we computed for all numerical runs in both cities the relation between the volume created by instabilities and the volume added to the numerical domain during a 1h time frame.

In the case of the city with a smooth gradient (Reynosa), the numerical model showed a great stability as no mass creation was determined in any run (using all the DEMs).

Whereas, in the city with steeper gradients (Saltillo), there was a small amount of water created by numerical instabilities. For instance, in the numerical run using the ASTER and SRTM DEMs, the errors where reported smaller than 0.005% for each hour time-step. Remarkably, the simulation using the AW3D30 DEM, reported errors of the same magnitude than those registered in numerical runs using both LiDAR derived datasets DSM and DTM (smaller than 0.5 %). In these cases, peak

values of this added volume were registered to be smaller than 1.0 %. Therefore, the amount of error associated to these instabilities is considered acceptable.

3.2.2 Qualitative analysis of water depth maps

In both cities, a qualitative analysis of the numerical results was deemed necessary, as there were clear differences between results in the numerical runs using the selected DEMs.

This was especially true in the results of the region with smoother slope (Reynosa), which are illustrated in Fig. 3. Different panels in this Figure show flood maps corresponding to the water depths registered at the end of the simulation time. Clearly and naturally, the less noisy output is obtained with the LiDAR derived DTM, which is our reference to reality. The smoothness of the solution degrades with each product in the following order: the LiDAR derived DSM, the AW3D30 DEM and the SRTM DEM. Numerical results using the ASTER DEM, provide a very noisy picture of this variable, indicating the little use of this dataset for this region as no clear flow path is distinguishable. These results are in accordance to those obtained in the comparison of slope and aspect.

Figure 4 introduces the same flood maps but determined at the end of the simulation time for the city of Saltillo, which is a region characterised by steeper slopes. In this case, similar results are obtained. However, in the case of the ASTER DEM the outcome the flow paths appear more clearly.

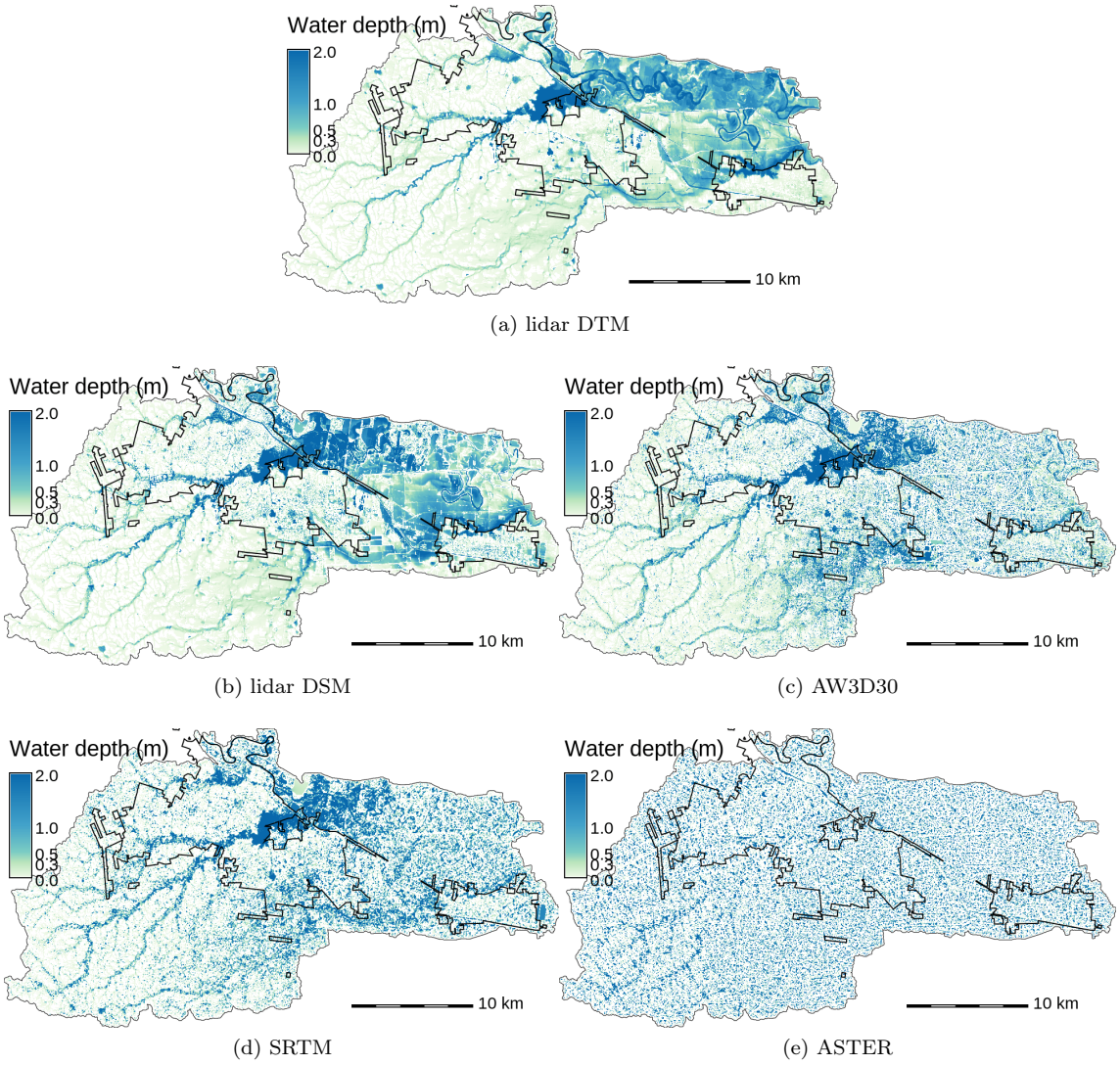

(a) lidar DTM

(b) lidar DSM

(c) AW3D30

(d) SRTM

(e) ASTER

Figure 3: Water levels at the end of the simulations in the flat catchment of Reynosa.

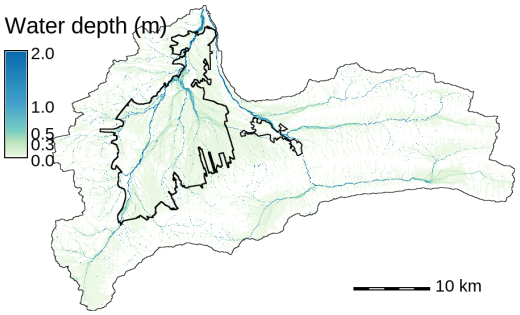

(a) lidar DTM

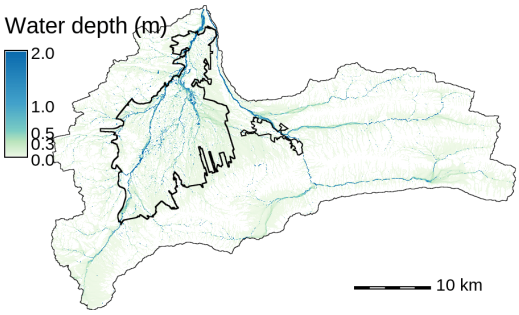

(b) lidar DSM

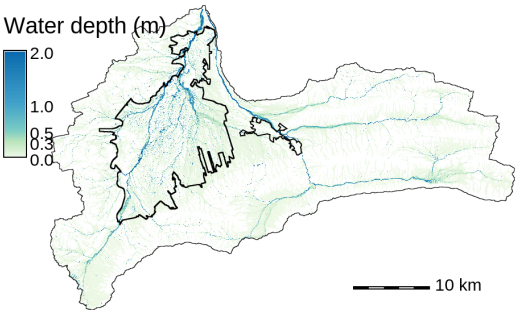

(c) AW3D30

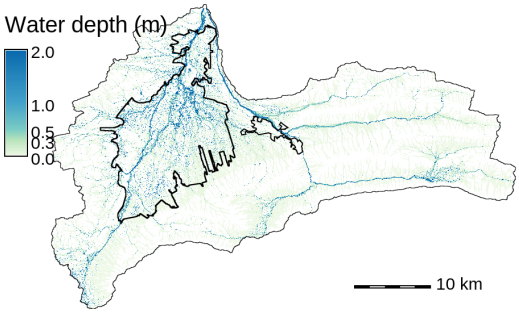

(d) SRTM

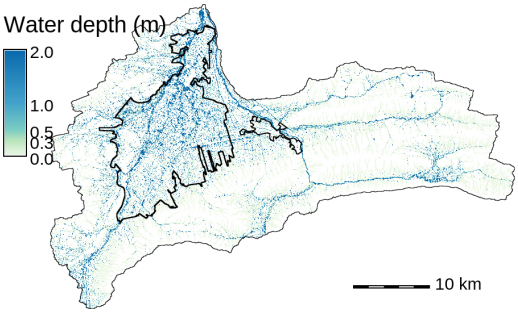

(e) ASTER

Figure 4: Water levels at the end of the simulations in the hilly catchment of Saltillo.

3.2.3 Time evolution of water volume within the domain

Another way to revise the quality of the DEM, is through the monitoring of the water volume and outflow within the domain. The noise of the DEM is reflected in the length of the time the model takes to reach an equilibrium state, i.e when the water volume exiting the domain become equal to the volume entering it. The noise in the elevation data affects the natural hydraulic connectivity in the study region, by for example creating artificial sinks that do not exist in reality.

Top panels of Figure 5 represent for both cases (smooth - left and steep - right gradient) the time evolution of water volume within the domain. While bottom panels introduce the time series of the outflow recorded exiting the domain in both areas. It is acknowledged that when the outflow and the domain volume stabilise, the numerical run has reached an equilibrium state (given the uniform forcing conditions). For this exercise, we consider that the model stabilise when the net addition to the domain volume falls under $1\,\mathrm{hm^3\,h^{-1}}$. Moreover, bottom panels in Fig. 5 allows us to estimate the time at which the flood wave reaches the outlet of the catchment. It is clear that in the case of city with steeper gradient (right bottom panel), the propagation of the flood wave is quicker than that observed in the smoother gradient case with a value smaller than 6 hours.

Remarkably, in the case of the region with steeper slopes, Saltillo, the two LiDAR derived DEMs and the AW3D30 DEM show a very similar behaviour of the flood wave, with arrival times between 5 to 6 hours and a stabilisation time within the range between 8 to 9 hours. In contrast, results for the SRTM DEM and the ASTER DEM show a clear deviation in the time evolution of both variables (volume and outflow), which casts some doubt in their adequacy for flood modelling in such study region. Moreover, the registered flood wave propagation times to the outflow point, are in accordance with the concentration time (8.5 hours) estimated through the Kirpich formula (See Table 1).

In the case of the numerical results using the SRTM DEM, the first flood wave arrives one hour later but does not stabilise until 19 h. This fact produces a flood volume almost twice as big as that registered in the numerical results using the LiDAR DTM ($77\,\mathrm{hm^3}$ versus $143\,\mathrm{hm^3}$). Similarly, numerical results obtained with the ASTER DEM, produce a propagation time of 15 h and a stabilisation time of 43 h,which produce a flood volume that is 4 times larger than that obtained in the numerical run using the LiDAR derived DTM ($77\,\mathrm{hm^3}$ versus $303\,\mathrm{hm^3}$).

On the other hand, results obtained in the region with smoother gradients indicated that for the simulation with the LiDAR derived DTM, the flood wave requires a larger time before reaching equilibrium given by 41 h. Indeed, none of the simulations ran with the selected global DEMs reaches the equilibrium. The numerical results using the AW3D30 DEM and the SRTM DEM show the start of a significant outflow around 38 h and 40 h, respectively. Lastly, simulation results obtained with the ASTER GDEM show no hydraulic connectivity, as no outflow is recorded exiting the domain in the 48 hours (maximum of $0.3\,\mathrm{hm^3}$).

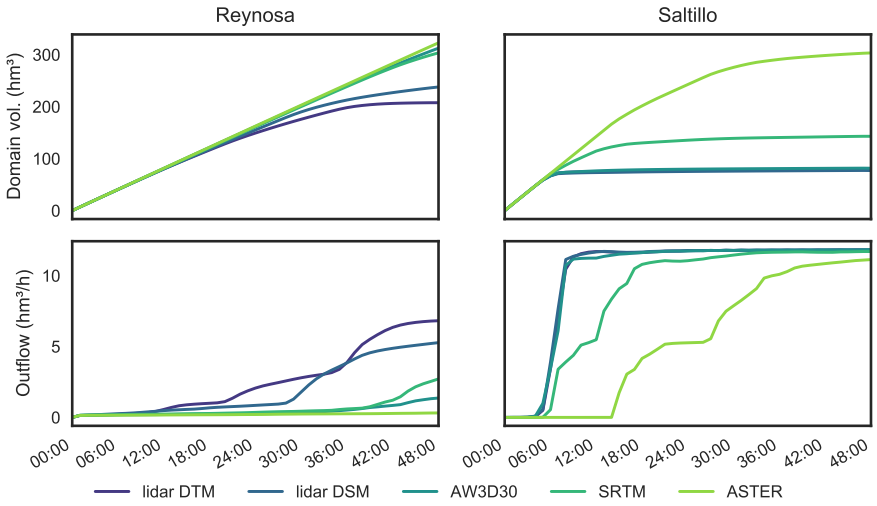

Figure 5: Time evolution of the water volume and outflow in the two observed computational domains.

3.2.4 Comparison of simulated water depths

A key variable in the validation of model results, when simulating floods is the total water depth. This variable is important to determine the level of damage that may be ascribed to a flood event, as it is utilised in the definition of flood hazard levels within a city or catchment.

Therefore, numerical results of this variable are also compared in both cases. Once again, reference values are determined through the results of the simulation using the LiDAR based DTM.

The results of this exercise are presented in Fig. 6, where left panel shows the results for the smooth gradient region (Reynosa) and the right panel introduces the results for the region with steep gradient (Saltillo). Results in both regions are classified in relation to the spatial location of the point of analysis (e.g. non-urban, urban and whole). This is done in order to analyse further whether there is a difference in the performance in the model in urban areas of the region.

As expected, in both selected cities, the DEM with the best performance (smaller error), is given by the LiDAR derived DSM. Notably, the second best dataset is the ALOS AW3D30 DEM, with a mean absolute error in the water depths that is in the order of that registered to the LiDAR DSM in the steep gradient case (Saltillo). Additionally, in this catchment, the errors in all DEMs are proved to be higher in the urban area than outside of it. This could be explained by two factors. First, the city is situated in an area of lower slopes, compared to the mountain range that comprises a large part of the non-urban area. This means that the DEM errors could be compensated by the higher slopes and hence are less noticeable. Second, it is known that urban areas are challenging for surface models, mainly due to the noise introduced by the sensors echo on the buildings.

In contrast, in the smooth gradient city (Reynosa), the skill of the AW3D30 DEM is not as good as that observed with the LiDAR derived DSM. Indeed, errors registered by the ALOS AW3D30 DEM in this case, are in the same order of magnitude as those registered with the SRTM DEM. Conversely, there no significant differences in the levels of errors between urban and non-urban areas in Reynosa. This could be due to the higher percentage of urbanised area (26 % versus 19 %, see Table 1) and that there is no strong changes of slopes between the non-urban and urban areas.

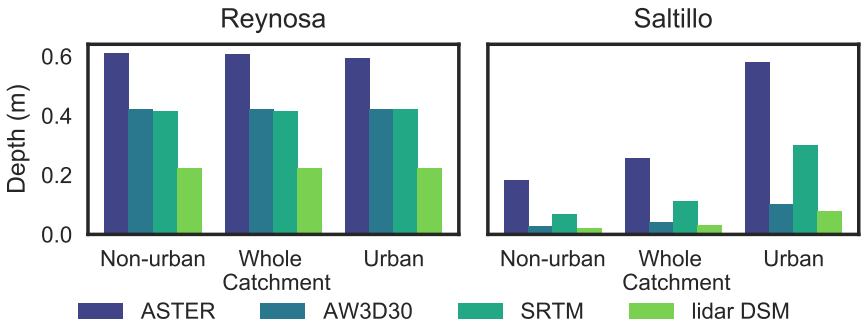

Figure 6: Mean Absolute Error in maximum water depth for each DEMs compared to the lidar DTM. Only values above 20cm are taken into account. Lower is better.

3.2.5 Comparison of flood extent

Finally, the last numerical result that is incorporated in the discussion is that related to the affected area by the flood in each numerical run. Therefore, an evaluation of the differences in flood extent maps is carried out. For this, we compute the Critical Success Index (CSI) [Stanski et al., 1989] determined by comparing the numerical result of each model run (AW3D30, SRTM, ASTER adn LidAR DSM) and city (Reynosa and Saltillo) against that obtained with the LidaR derived DTM.

Figure 7 presents for both selected cities, the CSI values for each nuemerical run using the different DEMs. In accordance to the results related to water depths, the LiDAR derived DSM presents the best skill of all DEMs analysed, while the ASTER DEM has very low values of CSI in both cases, indicating the poor suitability for its utilisation "as is" in flood modelling studies.

Right panel in Figure 7 summarises the results for the steep gradient region (Saltillo), where the AW3D30 is proven to be the best dataset when comparing flood extent results against the

other open global DEMs. Computed CSI values range between 0.40 and 0.61 and are within 0.1 of those obtained with the LiDAR derived DSM. In this catchment, it is noticeable that the CSI is reduced when moving from the non-urban area to the urban area, which is coherent with the results obtained when observing the water depth (see Fig. 6).

On the other hand, in the smooth gradient region of the city of Reynosa, numerical results indicate a degradation of the skill when using the AW3D30 DEM. Indeed, the CSI values computed with this DEM are again in accordance to those computed using the results of the SRTM DEM. This may indicate that in regions with smooth gradients the performance of the AW3D30 is similar to that registered usig the SRTM.

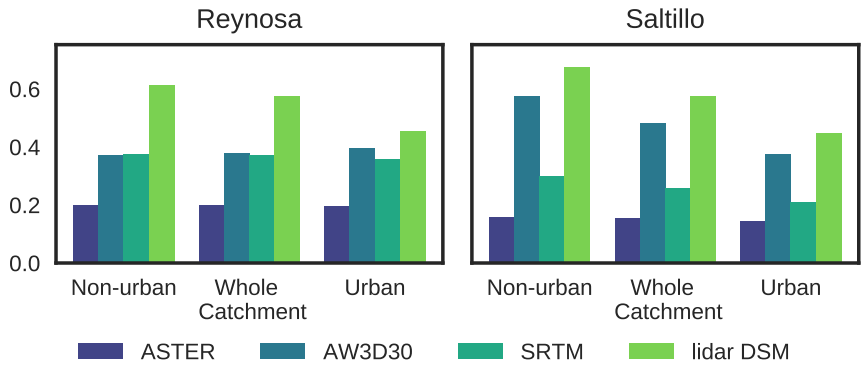

Figure 7: Critical Success Index calculated against the flood extent obtained with the lidar DTM. A cell is considered flooded when the water depth is above 20 cm. Perfect score is 1.

4 Discussion

Our results show that the AW3D30 is a welcome addition to the body of open-access global DEMs. Notably, in hilly areas characterised by steep gradients, the AW3D30 displays a clear improvement over the SRTM with performances in computer flood modelling that approach those obtained with a lidar DSM at the same horizontal resolution. This advantage is reduced in smooth gradient areas, but in this case, numerical results obtained with the AW3D30 DEM are at least as good as those registered using the SRTM DEM. However, some pending issues still need to be addressed.

First, the accuracy of global DEMs depends largely on the number of passes of the spacecraft above a given region and the usability of the collected data, for example due to cloud cover. The higher the number of passes and the lower the cloud cover, the higher the quality. There is indeed a spatial variability in the quality and availability of the same product. The present work describes results obtained in the north-east of Mexico and thus might not be representative of the accuracy of the studied DEM in all regions of the world. Hence, it would be valuable to perform such an evaluation of the AW3D30 in other parts of the planet. Moreover, herein we evaluate the version of the AW3D30 obtained through the arithmetic mean aggregation of the commercial AW3D at 5m. Some more work is needed to evaluate the differences that may occur by using the version obtained from the median aggregation. Finally, the AW3D30 is still a DSM, and therefore it includes noise and bias due to tree cover and buildings.

We see that AW3D30 does not address all the issues reproached to open-access global DEMs [Schumann et al., 2014, Simpson et al., 2015, Sampson et al., 2016]. Nevertheless, it is a clear improvement compared to the SRTM DEM, especially in areas of higher slopes. When possible, this DEM may replace the SRTM as a base for hydraulic conditioning that would further improve its performance when used in computer flood modelling, like it has been done with other products [Lehner et al., 2008, Jarihani et al., 2015, O'Loughlin et al., 2016, Yamazaki et al., 2017]. This would pave the way to an increase in accuracy of global flood models [Trigg et al., 2016] and in risk mapping in data-scarce countries.

5 Conclusions

Elevation datasets are acknowledged to play a significant role in hydrologic and hydraulic modelling of flood events. Modeover, flood inundation maps represent a key piece of information in preventing and reducing losses, as they enable the dissemination of flood risk to the society and decision makers (Rodríguez-Rincón et al. 2015).

However, good quality and accurate Digital Elevation Models are not availalable in all regions of the world.

In this paper we evaluated the suitability of the AW3D30 for computer flood modelling. We compared it with DSM and DTM obtained from aerial lidar and to other open-access global DEM at the same resolution of $1''$: the SRTM and the ASTER GDEM. In higher slopes, the AW3D30 performs better than the SRTM in every metrics. In lower slopes, the improvement is still present although lighter.

Similar evaluation needs to be done in other part of the world to confirm the encouraging proposition of the AW3D30. Additional investigation is needed to assess the possible differences between the median and mean versions of the product. Finally, further work might focus on the production of a hydrologically conditioned elevation model based on the AW3D30.

Acknowledgements

Laurent Courty is supported by a full doctoral scholarship from the UNAM's coordination of postgraduate studies.

Competing interests

The authors declare no conflict of interest.

References

Paul D. Bates. Remote sensing and flood inundation modelling. *Hydrological Processes*, 18(13):2593–2597, 9 2004. ISSN 0885-6087. doi: 10.1002/hyp.5649. URL `http://doi.wiley.com/10.1002/hyp.5649`.

David M Cobby, David C Mason, and Ian J Davenport. Image processing of airborne scanning laser altimetry data for improved river flood modelling. *ISPRS Journal of Photogrammetry and Remote Sensing*, 56(2):121–138, 12 2001. ISSN 09242716. doi: 10.1016/S0924-2716(01)00039-9.

Aaron Cook and Venkatesh Merwade. Effect of topographic data, geometric configuration and modeling approach on flood inundation mapping. *Journal of Hydrology*, 377 (1-2):131–142, 10 2009. ISSN 00221694. doi: 10.1016/j.jhydrol.2009.08.015. URL `http://linkinghub.elsevier.com/retrieve/pii/S0022169409004909`.

Laurent Guillaume Courty, Adrián Pedrozo-Acuña, and Paul David Bates. Itzï (version 17.1): an open-source, distributed GIS model for dynamic flood simulation. *Geoscientific Model Development*, 10(4):1835–1847, 5 2017. doi: 10.5194/gmd-10-1835-2017. URL `http://www.geosci-model-dev.net/10/1835/2017/`.

Gustavo A. M. de Almeida and Paul David Bates. Applicability of the local inertial approximation of the shallow water equations to flood modeling. *Water Resources Research*, 49(8):4833–4844, 2013. ISSN 00431397. doi: 10.1002/wrcr.20366.

Gustavo A. M. de Almeida, Paul David Bates, Jim E. Freer, and Maxime Souvignet. Improving the stability of a simple formulation of the shallow water equations for 2-D flood modeling. *Water Resources Research*, 48(5):1–14, 2012. ISSN 00431397. doi: 10.1029/2011WR011570.

Giuliano Di Baldassarre. Data sources. In *Floods in a Changing Climate: Inundation Modelling*, pages 33–42. Cambridge University Press, Cambridge. doi: 10.1017/CBO9781139088411.008. URL `http://ebooks.cambridge.org/ref/id/CBO9781139088411A013`.

Tom G. Farr, Paul A. Rosen, Edward Caro, Robert Crippen, Riley Duren, Scott Hensley, Michael Kobrick, Mimi Paller, Ernesto Rodriguez, Ladislav Roth, David Seal, Scott Shaffer, Joanne Shimada, Jeffrey Umland, Marian Werner, Michael Oskin, Douglas Burbank, and Douglas Alsdorf. The Shuttle Radar Topography Mission. *Reviews of Geophysics*, 45(2):RG2004, 5 2007. ISSN 8755-1209. doi: 10.1029/2005RG000183. URL http://doi.wiley.com/10.1029/2005RG000183.

T. J. Fewtrell, Paul David Bates, M. Horritt, and N. M. Hunter. Evaluating the effect of scale in flood inundation modelling in urban environments. *Hydrological Processes*, 22(26):5107–5118, 12 2008. ISSN 08856087. doi: 10.1002/hyp.7148. URL http://doi.wiley.com/10.1002/hyp.7148.

Humberto A. Gallegos, Jochen E. Schubert, and Brett F. Sanders. Two-dimensional, high-resolution modeling of urban dam-break flooding: A case study of Baldwin Hills, California. *Advances in Water Resources*, 32(8):1323–1335, 8 2009. ISSN 03091708. doi: 10.1016/j.advwatres.2009.05.008.

Dean B. Gesch, Michael J. Oimoen, and Gayla A. Evans. Accuracy assessment of the U.S. Geological Survey National Elevation Dataset, and comparison with other large-area elevation datasets: SRTM and ASTER. Technical report, 2014. URL https://pubs.er.usgs.gov/publication/ofr20141008.

Stephane Hallegatte, Colin Green, Robert J Nicholls, and Jan Corfee-Morlot. Future flood losses in major coastal cities. *Nature climate change*, 3(9):802–806, 2013. doi: 10.1038/nclimate1979.

Yukiko Hirabayashi, Roobavannan Mahendran, Sujan Koirala, Lisako Konoshima, Dai Yamazaki, Satoshi Watanabe, Hyungjun Kim, and Shinjiro Kanae. Global flood risk under climate change. *Nature Climate Change*, 3(9):816–821, 2013. ISSN 1758-678X. doi: 10.1038/nclimate1911. URL http://www.nature.com/doifinder/10.1038/nclimate1911.

C. Hirt, M. S. Filmer, and W. E. Featherstone. Comparison and validation of the recent freely available ASTER-GDEM ver1, SRTM ver4.1 and GEODATA DEM-9S ver3 digital elevation models over Australia. *Australian Journal of Earth Sciences*, 57 (3):337–347, 4 2010. ISSN 0812-0099. doi: 10.1080/08120091003677553. URL http://www.tandfonline.com/doi/abs/10.1080/08120091003677553.

Michael E. Hodgson and Patrick Bresnahan. Accuracy of Airborne Lidar-Derived Elevation. *Photogrammetric Engineering & Remote Sensing*, 3:331–339, 2004. ISSN 00991112. doi: 10.14358/PERS.70.3.331.

M.S Horritt and P.D Bates. Effects of spatial resolution on a raster based model of flood flow. *Journal of Hydrology*, 253(1-4):239–249, 11 2001. ISSN 00221694. doi: 10.1016/S0022-1694(01)00490-5. URL http://linkinghub.elsevier.com/retrieve/pii/S0022169401004905.

Arthur Y. Hou, Ramesh K. Kakar, Steven Neeck, Ardeshir A. Azarbarzin, Christian D. Kummerow, Masahiro Kojima, Riko Oki, Kenji Nakamura, and Toshio Iguchi. The Global Precipitation Measurement Mission. *Bulletin of the American Meteorological Society*, 95(5):701–722, 5 2014. ISSN 0003-0007. doi: 10.1175/BAMS-D-13-00164.1. URL http://journals.ametsoc.org/doi/abs/10.1175/BAMS-D-13-00164.1.

IFRC. *World Disasters Report 2016. Resilience : saving lives today, investing for tomorrow.* 2016. ISBN 9789291392407. URL http://www.ifrc.org/en/publications-and-reports/world-disasters-report/world-disasters-report/.

Abdollah A. Jarihani, John N. Callow, Tim R. McVicar, Thomas G. Van Niel, and Joshua R. Larsen. Satellite-derived Digital Elevation Model (DEM) selection, preparation and correction for hydrodynamic modelling in large, low-gradient and data-sparse catchments. *Journal of Hydrology*, 524:489–506, 2015. ISSN 00221694. doi: 10.1016/j.jhydrol.2015.02.049.

Changwei Jing, Ashton Shortridge, Shengpan Lin, and Jiaping Wu. Comparison and validation of SRTM and ASTER GDEM for a subtropical landscape in Southeastern China. *International Journal of Digital Earth*, 7(12): 969–992, 11 2014. ISSN 1753-8947. doi: 10.1080/17538947.2013.807307. URL http://www.tandfonline.com/doi/abs/10.1080/17538947.2013.807307.

T Kenward. Effects of Digital Elevation Model Accuracy on Hydrologic Predictions. *Remote Sensing of Environment*, 74(3):432–444, 12 2000. ISSN 00344257. doi: 10.1016/S0034-4257(00)00136-X.

Gina LeFavour and Doug Alsdorf. Water slope and discharge in the Amazon River estimated using the shuttle radar topography mission digital elevation model. *Geophysical Research Letters*, 32(17), 9 2005. ISSN 00948276. doi: 10.1029/2005GL023836. URL http://doi.wiley.com/10.1029/2005GL023836.

Bernhard Lehner, Kristine Verdin, and Andy Jarvis. New Global Hydrography Derived From Spaceborne Elevation Data. *Eos, Transactions American Geophysical Union*, 89(10):93, 3 2008. ISSN 0096-3941. doi: 10.1029/2008EO100001. URL http://doi.wiley.com/10.1029/2008EO100001.

Kate Marks and Paul Bates. Integration of high-resolution topographic data with floodplain flow models. *Hydrological Processes*, 14(11-12):2109–2122, 8 2000. ISSN 0885-6087. doi: {10.1002/1099-1085(20000815/30)14:11/12<2109::AID-HYP58>3.0.CO;2-1}.

Vorawit Meesuk, Zoran Vojinovic, Arthur E. Mynett, and Ahmad F. Abdullah. Urban flood modelling combining top-view LiDAR data with ground-view SfM observations. *Advances in Water Resources*, 75:105–117, 1 2015. ISSN 03091708. doi: 10.1016/j.advwatres.2014.11.008.

Helena Mitášová and Lubos Mitáš. Interpolation by regularized spline with tension: I. Theory and implementation. *Mathematical Geology*, 25(6):641–655, 1993. ISSN 08828121. doi: 10.1007/BF00893171.

F.E. O'Loughlin, R.C.D. Paiva, M. Durand, D.E. Alsdorf, and P.D. Bates. A multi-sensor approach towards a global vegetation corrected SRTM DEM product. *Remote Sensing of Environment*, 182:49–59, 9 2016. ISSN 00344257. doi: 10.1016/j.rse.2016.04.018. URL http://linkinghub.elsevier.com/retrieve/pii/S0034425716301821.

A. Pedrozo-Acuña, J.P. Rodríguez-Rincón, M. Arganis-Juárez, R. Domínguez-Mora, and F.J. González Villareal. Estimation of probabilistic flood inundation maps for an extreme event: Pánuco River, México. *Journal of Flood Risk Management*, 8(2):177–192, 6 2015. ISSN 1753318X. doi: 10.1111/jfr3.12067. URL http://doi.wiley.com/10.1111/jfr3.12067.

Adrián Pedrozo-Acuña, I Mariño-Tapia, C Enriquez, Gabriela Medellín Mayoral, and Fernando J. González Villareal. Evaluation of inundation areas resulting from the diversion of an extreme discharge towards the sea: case study in Tabasco, Mexico. *Hydrological Processes*, 26(5):687–704, 2 2012. ISSN 08856087. doi: 10.1002/hyp.8175. URL http://doi.wiley.com/10.1002/hyp.8175.

M. Rexer and C. Hirt. Comparison of free high resolution digital elevation data sets (ASTER GDEM2, SRTM v2.1/v4.1) and validation against accurate heights from the Australian National Gravity Database. *Australian Journal of Earth Sciences*, 61 (2):213–226, 2 2014. ISSN 0812-0099. doi: 10.1080/08120099.2014.884983. URL http://www.tandfonline.com/doi/abs/10.1080/08120099.2014.884983.

Christopher C. Sampson, Andrew M. Smith, Paul David Bates, Jeffrey C. Neal, and Mark A. Trigg. Perspectives on Open Access High Resolution Digital Elevation Models to Produce Global Flood Hazard Layers. *Frontiers in Earth Science*, 3:85, 1 2016. ISSN 2296-6463. doi: 10.3389/feart.2015.00085. URL http://journal.frontiersin.org/Article/10.3389/feart.2015.00085/abstract.

Brett F. Sanders. Evaluation of on-line DEMs for flood inundation modeling. *Advances in Water Resources*, 30(8):1831–1843, 8 2007. ISSN 03091708. doi: 10.1016/j.advwatres.2007.02.005. URL http://linkinghub.elsevier.com/retrieve/pii/S0309170807000279.

J. R. Santillan and M. Makinano-Santillan. Vertical Accuracy Assessment of 30-M Resolution Alos, Aster, and Srtm Global Dems Over Northeastern Mindanao, Philippines. *International Archives of the Photogrammetry, Remote Sensing and Spatial Information Sciences*, XLI-B4(July), 2016. ISSN 2194-9034. doi: 10.5194/isprsarchives-XLI-B4-149-2016.

G. Schumann, G. Di Baldassarre, D. Alsdorf, and P. D. Bates. Near real-time flood wave approximation on large rivers from space: Application to the River Po, Italy. *Water Resources Research*, 46(5), 5 2010. ISSN 00431397. doi: 10.1029/2008WR007672.

Guy Jean-Pierre Schumann, Paul David Bates, Jeffrey C. Neal, and Konstantinos M. Andreadis. Fight floods on a global scale. *Nature*, 507(7491):169–169, 3 2014. doi: 10.1038/507169e. URL http://www.nature.com/doifinder/10.1038/507169e.

Alanna L. Simpson, Simone Balog, Delwyn K. Moller, Benjamin H. Strauss, and Keiko Saito. An urgent case for higher resolution digital elevation models in the world's poorest and most vulnerable countries. *Frontiers in Earth Science*, 3:50, 8 2015. ISSN 2296-6463. doi: 10.3389/feart.2015.00050. URL http://journal.frontiersin.org/Article/10.3389/feart.2015.00050/abstract.

Henry R Stanski, Laurence J Wilson, and William R Burrows. *Survey of common verification methods in meteorology*. World Meteorological Organization Geneva, 1989.

Tetsushi Tachikawa, Masami Hato, Manabu Kaku, and Akira Iwasaki. Characteristics of ASTER GDEM version 2. In *2011 IEEE International Geoscience and Remote Sensing Symposium*, pages 3657–3660. IEEE, 7 2011. ISBN 978-1-4577-1003-2. doi: 10.1109/IGARSS.2011.6050017. URL http://ieeexplore.ieee.org/document/6050017/.

T. Tadono, H. Nagai, H. Ishida, F. Oda, S. Naito, K. Minakawa, and H. Iwamoto. GENERATION OF THE 30 M-MESH GLOBAL DIGITAL SURFACE MODEL BY ALOS PRISM. *ISPRS - International Archives of the Photogrammetry, Remote Sensing and Spatial Information Sciences*, XLI-B4:157–162, 6 2016. ISSN 2194-9034. doi: 10.5194/isprs-archives-XLI-B4-157-2016. URL http://www.int-arch-photogramm-remote-sens-spatial-inf-sci.net/XLI-B4/157/2016/.

Tesfaye Haimanot Tarekegn, Alemseged Tamiru Haile, Tom Rientjes, P. Reggiani, and Dinand Alkema. Assessment of an ASTER-generated DEM for 2D hydrodynamic flood modeling. *International Journal of Applied Earth Observation and Geoinformation*, 12(6):457–465, 12 2010. ISSN 03032434. doi: 10.1016/j.jag.2010.05.007. URL http://linkinghub.elsevier.com/retrieve/pii/S0303243410000620.

M A Trigg, C E Birch, J C Neal, P D Bates, A Smith, C C Sampson, D Yamazaki, Y Hirabayashi, F Pappenberger, E Dutra, P J Ward, H C Winsemius, P Salamon, F Dottori, R Rudari, M S Kappes, A L Simpson, G Hadzilacos, and T J Fewtrell. The credibility challenge for global fluvial flood risk analysis. *Environmental Research Letters*, 11(9):094014, 9 2016. ISSN 1748-9326. doi: 10.1088/1748-9326/11/9/094014. URL http://stacks.iop.org/1748-9326/11/i=9/a=094014?key=crossref.b898d75acc25c871d21b6be9b2ebcd65.

Weicai Wang, Xiaoxin Yang, and Tandong Yao. Evaluation of ASTER GDEM and SRTM and their suitability in hydraulic modelling of a glacial lake outburst flood in southeast Tibet. *Hydrological Processes*, 26(2):213–225, 1 2012. ISSN 08856087. doi: 10.1002/hyp.8127. URL http://doi.wiley.com/10.1002/hyp.8127.

Dai Yamazaki, Daiki Ikeshima, Ryunosuke Tawatari, Tomohiro Yamaguchi, Fiachra O'Loughlin, Jeffery C. Neal, Christopher C. Sampson, Shinjiro Kanae, and Paul D. Bates. A high-accuracy map of global terrain elevations. *Geophysical Research Letters*, 44(11):5844–5853, 6 2017. ISSN 00948276. doi: 10.1002/2017GL072874. URL http://doi.wiley.com/10.1002/2017GL072874.

Kun Yan, Giuliano Di Baldassarre, Dimitri P. Solomatine, and Guy J.-P. Schumann. A review of low-cost space-borne data for flood modelling: topography, flood extent and water level. *Hydrological Processes*, 29(15):3368–3387, 7 2015a. ISSN 08856087. doi: 10.1002/hyp.10449. URL http://doi.wiley.com/10.1002/hyp.10449.

Kun Yan, Angelica Tarpanelli, Gabor Balint, Tommaso Moramarco, and Giuliano Di Baldassarre. Exploring the Potential of SRTM Topography and Radar Altimetry to Support Flood Propagation Modeling: Danube Case Study. *Journal of Hydrologic Engineering*, 20(2):04014048, 2 2015b. ISSN 1084-0699. doi: 10.1061/(ASCE)HE.1943-5584.0001018.